Analyst

PAPER

View Article Online
View Journal

Cite this: DOI: 10.1039/d6an00114a

A portable acoustic biosensing platform combined with paper-based capillary fluidics for the rapid detection of antibodies in serum

Dimitra Chronaki, [a] Stylianos Grammatikos, †[a,b] Angelos Ntimtsas, †[a] Marios Matsis,[b] Orestis F. Kokolakis,[b] Konstantina Alexaki, [a] Zoi Pournara,[c] Achilleas Tsortos, [a] Alexandros Zafiropoulos [c] and Electra Gizeli *[a,b]

We report the development of a sensitive biosensing platform based on a shear-horizontal surface acoustic wave (SH-SAW) device and paper fluidics, with the potential to be used outside centralized laboratory settings. Systematic research on the biorecognition surface, blocking agent, fluidics and measuring unit allowed us to transform a laboratory-based method into a field-deployable device. As a proof-of-concept, the platform was used for the detection of SARS-CoV-2 anti-spike antibodies on a surface-immobilized spike protein, tested in both simulated and human blood serum samples. A poly-L-lysine (PLL) layer was selected as a biocompatible surface for spike protein immobilization; the polymer layer can be easily removed through gentle mechanical rubbing, allowing regeneration and multiple uses of the sensing device. This surface, combined with novel paper-based capillary fluidics, enabled real-time monitoring of spike antibody binding *via* acoustic wave phase measurements in the range of 1–100 nM antibodies in 1% v/v serum. Further acoustic wave amplitude amplification and a tenfold improvement in the detection limit (0.1 nM) were achieved by the use of gold nanoparticles conjugated with a secondary antibody. This optimized assay was successfully evaluated in a small pilot clinical study of 20 patient samples. Our new SH-SAW immunosensor exhibited sensitivity and specificity comparable to commercial systems with standard fluidics and instrumentation; importantly, its limit of detection is better than the clinically relevant value of ~11 RU mL^{-1}. This portable, low-cost platform, combining a pocket-size network analyzer with disposable paper fluidics and a regenerable sensing surface, offers a promising solution for quantitative antibody detection near or at the point-of-care.

Received 30th January 2026,
Accepted 18th April 2026

DOI: 10.1039/d6an00114a

rsc.li/analyst

Introduction

The development of portable, robust and reliable devices for the analysis of biomarkers in human samples outside a dedicated laboratory is one of the current priorities in diagnostics and healthcare as witnessed by the huge shift from laboratory testing to the point-of-care (POC).[1] International non-profit organizations such as the World Health Organization (WHO) and the Foundation for Innovative New Diagnostics (FIND) have declared the development of affordable, accessible and simple to operate diagnostic tests, an area of strategic research priority, specifically for the management of poverty-related diseases in low- and middle-income countries. However, there are several analytical and engineering challenges related to the development of efficient diagnostic tools for field detection. High specificity and sensitivity towards the analyte of interest, combined with portable detection instrumentation amenable to miniaturization, are fundamental for testing outside a laboratory. In addition, rapid analysis (~30 min), simplicity in operation (one or two steps) and low cost (few $ per test) are key criteria for the development of global diagnostic tools for POC applications.[2] As a result, during the last few years, there has been a shift towards the development of paper-based technologies for rapid testing at the POC due to their simplicity and wide applicability.[3]

Lateral flow immunoassays (LFIAs), currently the gold standard for POC testing,[4] are used for the rapid detection of either antigens (Ag) or antibodies (Ab) in human samples. The technology became widely applicable during the pandemic for rapid COVID-19 home testing.[5] However, while the LFIAs are fast, user-friendly, low-cost and with minimal sample pretreat-

[a]*Institute of Molecular Biology and Biotechnology, Foundation for Research and Technology-Hellas, Heraklion, Crete 70013, Greece. E-mail: gizeli@imbb.forth.gr*
[b]*Department of Biology, University of Crete, Heraklion, Crete 70013, Greece*
[c]*Laboratory of Clinical Virology, Medical School, University of Crete, Heraklion, Crete 71003, Greece*
† These authors contributed equally to this work.

ment requirements, they provide mostly qualitative results; semi-quantitative results can also be obtained in combination with lateral flow readers or naked-eye estimations.[6–8] Qualitative detection has limitations, including faint bands in the case of a low-affinity Ab and very strong (occasionally non-specific) bands in the case of a low specificity Ab, both of which are assessed by the naked eye. Furthermore, other challenges include problems in reproducibility and multiplexing.[9,10] To address these limitations, combinations of paper-based LFIAs with sensing technologies such as electrochemical biosensors have been explored, producing electrofluidic platforms that embed electrodes into paper for enhanced biosensing applications.[11–13]

Acoustic biosensors have been used extensively for antibody/antigen detection in immunosensing applications. Shear-horizontal surface acoustic wave (SH-SAW) devices, in particular, have several applications due to their planar geometry enabling integration with microfluidics, heating elements and lab-on-a-chip technologies.[14–20] SH-SAW devices can provide label-free and real-time quantitative results through the monitoring of the phase and amplitude of the acoustic wave. So far, their applications include the detection of Ab,[21–25] Ag[26,27] and protein biomarkers.[28–30] Specifically, the detection of Ab was demonstrated in buffer[22,24] or complex samples including plasma,[21,24] serum[23] and whole blood[25] for various targets such as SARS-CoV-2,[23,25] HIV[24] and hepatitis B[31] antigens. Typical reported detection limits for Ab are in the range of nM (ref. 24) to pM.[22,23] Moreover, some studies have used nanomaterials,[32] such as streptavidin-coated gold nanoparticles (AuNPs),[27,33] Ab-conjugated AuNPs[23,28] and gold staining,[28] to further amplify the acoustic signal as a result of the added mass effect. Despite these achievements, the development of a field-deployable SAW platform for immunosensing remains a challenge.

Recently, our group reported the combination of a portable SH-SAW analyzer with a novel paper-strip capillary fluidic system.[34] That removable strip was used for liquid medium transfer over the sensing area, replacing the traditional polymeric surface-sealed (micro)fluidic cell; it was positioned on top of the device to form the upper boundary of a capillary flow channel. With that set up, we efficiently detected various concentrations of glycerol and DNA (a ladder) as a proof-of-concept. Here, we advance the technology further by investigating its applicability as an immunosensor, using SARS-CoV-2 Ab in serum samples as a model target. To achieve optimal results, we studied and optimized the effect of all relevant components of a biosensor, *i.e.*, the biorecognition layer, flow cell geometry and measuring unit. The poly-L-lysine (PLL) layer was selected for the immobilization of the spike protein since it enables surface regeneration/cleaning on the spot.[34] Using human serum samples already tested for the presence or absence of anti-spike Ab *via* ELISA, we showed excellent discrimination capability (100% detection) between four negative and sixteen positive samples, in agreement with the ELISA results. Moreover, a further increase in the signal response by 2 (phase) and 3 (amplitude) times was observed when AuNPs functionalized with a secondary Ab were added on the device surface. Finally, through systematic investigation and comparison of standard and novel mechanical, fluidic and electrical components, we showed that the paper-strip fluidics combined with a portable measuring unit could form an attractive platform for near or at the POC immune testing.

Materials and methods

Materials

Poly-L-lysine (PLL, M_w 150–300 kDa), bovine serum albumin (BSA), casein from bovine milk, gold(III) chloride trihydrate ($HAuCl_4 \cdot 3H_2O$, ≥49% Au basis), sodium citrate tribasic dihydrate (TCD), phosphate buffered saline (PBS) tablets and water for chromatography (LC-MS grade) were purchased from Merck (Germany). SARS-CoV-2 spike glycoprotein was obtained from Trenzyme, Germany (P2020-029). Rabbit anti-spike Ab from Sino Biological, China (40592-R001), goat anti-rabbit IgG Ab from Thermo Fisher, USA (SA510231), and goat anti-human IgG Fc from Abcam, UK (ab97221) were used. PBS tablets in deionized water yielded a 10 mM phosphate buffer with 2.7 mM KCl, 137 mM NaCl and pH 7.4 at 25 °C. All chemicals were used as received, without any further purification.

SAW device

Single-channel SAW devices (AWS SNS-000069-A, AWSensors, Spain) with a fundamental frequency of 120 MHz were fabricated on a 0.35 mm thick AT-cut quartz substrate with patterned interdigital transducers (IDTs) in a double-finger geometry (Fig. 1A). A Love-wave SAW device was created by depositing a 3 μm SiO_2 as a guiding layer on the sensing area. A gold (Au) (50 nm) layer, deposited on top of a thin Cr (10 nm) adhesion film between the IDTs, was used to create the biorecognition surface. Prior to biosensing experiments, the SAW sensors were treated with UV ozone (Ossila, UK) for 30 min. The following solutions were flowed onto the device surface at the beginning of each experiment: 2% Hellmanex (Sigma) and dH_2O for cleaning of the sensing area. At the end of each experiment, the device surface was also cleaned with 2% Hellmanex and dH_2O and dried under nitrogen flow. In the case where the surface was modified with PLL, the device-surface was regenerated after removing the PLL layer (and all proteins attached to it) with a cotton swab soaked first with dH_2O and then 70% v/v ethanol.

Laboratory-based fluidics and measuring platform

A commercial flow cell (AWS CLS-000028-A, AWSensors, Spain), with a cover of PSU (polysulfone) and a PDMS (polydimethylsiloxane) O-ring (Fig. 1B), was positioned on top of the device and between the IDTs,[35] and used with a flow control unit (FCU, AWSensors, Spain) to deliver the samples to the sensor surface. The flow cell was cleaned before and after each experiment with 2% Hellmanex, dH_2O and dried under nitrogen flow. The dimensions of the flow cell were 47 (L) × 33 (W) × 44 (H) mm and the chamber volume was 5.5 μL. A benchtop network analyzer (SENSeOR, France)[36] was further employed to record acoustic wave amplitude shifts (ΔA) and phase shifts

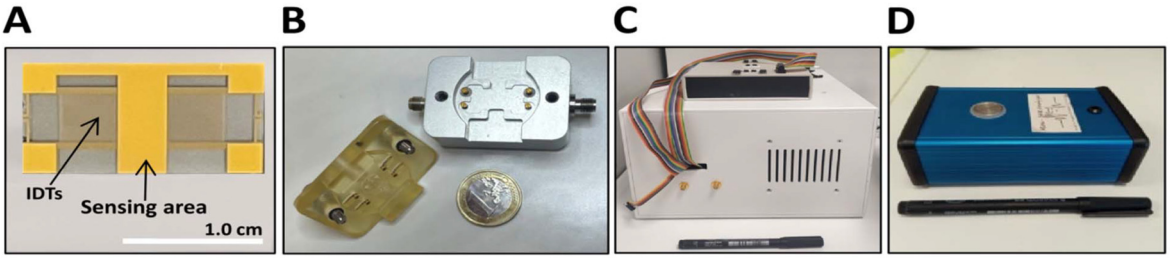

Fig. 1 Images of the device, flow cell and analyzers used: (A) 120 MHz SAW sensor, (B) AWS device holder and flow cell, (C) SENSeOR measuring unit and (D) in-house portable measuring unit.

(ΔPh), with the analyzer's dimensions being 25.5 (*L*) × 25.5 (*W*) × 16 (*H*) cm (Fig. 1C).

Portable acoustic platform

The Love-SAW sensor was further combined with a portable, in-house made measuring platform (Fig. 1D and 2A).[34] This hand-held device, with dimensions 13.8 (*L*) × 8 (*W*) × 5 (*H*) cm, was used to record amplitude and phase changes (in dB and deg units, respectively) (Fig. 1D). The measuring unit consisted of a programmable phase-locked loop (P-LL) oscillator, where the frequency was adjusted based on the working frequency of the SAW device. For amplitude and phase shift monitoring, a gain/phase detector was used. To reduce interfering reflections, square pieces of parafilm (3 × 2 mm) were placed on the edges of each IDT to act as absorbers.[34] A micropump (CPP-1 180-ZM, Jobst Technologies, Germany) and a pulse width modulated (PWM) controller were implemented to adjust the flow rate. Finally, a microcontroller was used to adjust the P-LL oscillator working frequency (depending on the SAW sensor in use), to read and report the values from the gain/phase detector to a personal computer and adjust the PWM duty cycle for the micropump. The sensor system was calibrated and ensured accurate measurements for both amplitude and phase, with a high resolution of 2.10 mdB and 6.10 mdeg and a low drift rate of 0.72 mdB h^{-1} and 1.00 mdeg h^{-1}, respectively.[34] The overall dimensions of the portable measuring platform were 22 (*L*) × 8 (*W*) × 5 (*H*) cm (Fig. 2A).

Paper-based capillary fluidics on SAW

The paper-based capillary concept is illustrated in Fig. 2A and B and described in detail in a previous work.[34] Briefly, a capil-

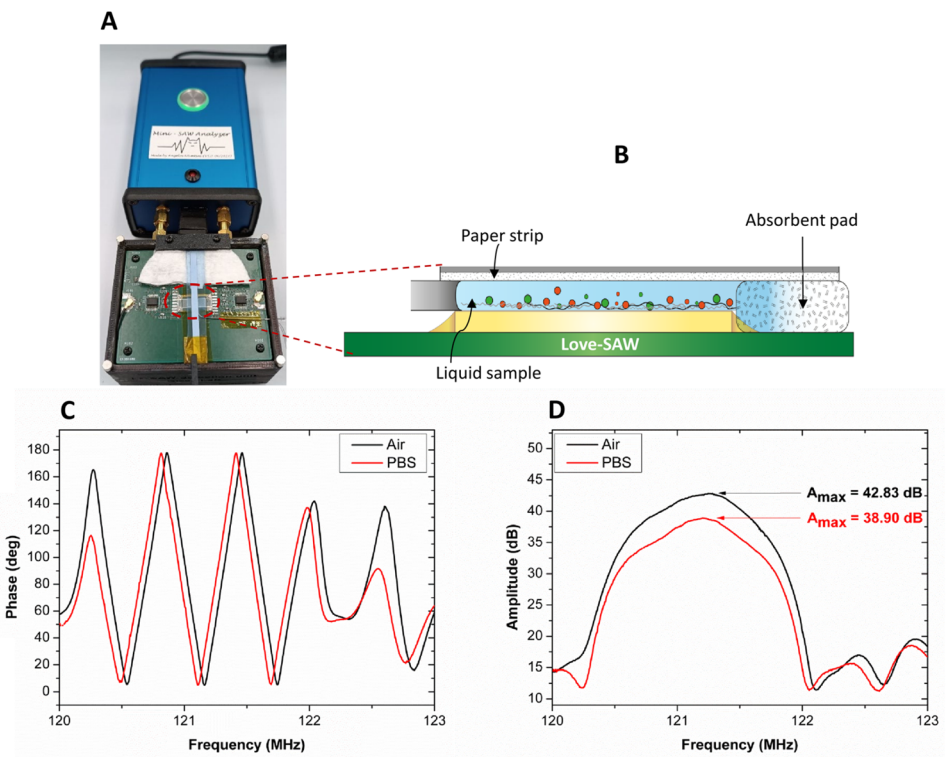

Fig. 2 (A) Image of the portable measuring platform, consisting of a mini-SAW analyzer and a SAW housing unit. (B) Schematic of the LFS placed above the SAW device, creating the capillary channel. (C) Phase and (D) amplitude signals of a 120 MHz sensor in air (black line) and PBS (red line).

lary channel was created on the surface of the SAW device using a paper nitrocellulose strip. To create the capillary, a commercial lateral flow strip (LFS) (Novatech, Turkey) was employed upon removing all pads from its surface by placing it at a 0.5 mm distance from the surface using a glass slide for support. This contactless flow cell structure minimized the energy losses normally observed during sealing of the flow cell to the device surface. It also resulted in a smooth amplitude response even in the presence of the liquid sample and a linear phase response (Fig. 2C and D). To enable the performance of a multi-step assay, including surface functionalization, sample testing, and/or signal amplification, the micropump was connected to a syringe that brought the sample to the inlet of the strip at a constant flow rate of 20 μL min^{-1}. In this way, we achieved continuous flow for more than an hour without leakage or collapse of the capillary. A cotton pad was finally placed at the end of the capillary channel as an absorbent pad.

The phase and amplitude signals of the 120 MHz sensor exposed in air and PBS buffer are shown in Fig. 2C and D. In the phase plot, there is a shift in phase values when moving from air to PBS measurements while the typical triagonal pattern is maintained. The maximum amplitude (A_{max}) value in air was 42.83 dB and 38.90 dB in PBS, while the peak shape was also maintained.

Anti-spike Ab binding isotherm on SAW

For SARS-CoV-2 spike protein binding, two different surfaces were utilized: the first employed the bare, negatively charged Au-coated (isoelectric point of ~5.2)[37] SAW device for the direct physisorption of the spike protein in PBS (0.06 mg mL^{-1}, V = 50 μL), followed by the addition of PBS containing BSA (1% w/v) or serum (1% v/v) as blocking agents. Serum obtained from a patient negative to COVID-19 was also used as a medium for the target Ab injection. The second surface was produced after applying a 0.01% w/v solution of PLL in PBS under flow onto the Au-SAW surface (V = 100 μL). The positively charged PLL surface was used to bind the spike protein (0.06 mg mL^{-1}, V = 50 μL) of negative charge (UniProt: P0DTC2, theoretical isoelectric point of ~6.24, calculated from Expasy ProtParam) leading to electrostatic immobilization, followed by the addition of casein (1% w/v solution in PBS) and serum (1% v/v in PBS) as blocking agents. Both spike-modified surfaces were employed for the sequential addition of increasing concentrations of rabbit anti-spike Ab (*i.e.*, 1, 2, 5, 10, 50 and 100 nM) in 1% v/v serum solutions (V = 60 μL of each injection) in PBS buffer. All experiments were performed at 25 °C and with a constant flow rate of 20 μL min^{-1}, while experiments were repeated at least three times.

Synthesis and bio-functionalization of TCD-AuNPs

Gold nanoparticles (AuNPs) with an average diameter of ~13 nm were synthesized using the Turkevich method with slight modifications.[38] For biofunctionalization, a secondary Ab (either goat anti-rabbit or goat anti-human IgG) solution at an optimized concentration was incubated with appropriate volumes of AuNP solutions (OD 1) at pH 9.0–9.5 for 1 h. Following passive adsorption of the secondary Ab ("2Ab") onto the AuNP surface, the AuNP-2Ab conjugates were purified, redispersed in PBS containing 0.1% w/v BSA, and stored at 4 °C until further use. The resulting bioconjugates were used within 3 weeks. The working concentration of the AuNPs (OD 1) employed in the experiments was estimated to be ~4.78 nM. Additional details on AuNP synthesis, biofunctionalization and characterization *via* UV-Vis absorbance, scanning electron microscopy (SEM) and transmission electron microscopy (TEM) are provided in the SI (SI and Fig. S1).

Signal amplification using QCM-D

A quartz crystal microbalance with dissipation monitoring (QCM-D),[39] an acoustic biosensor comprising a thin AT-cut quartz crystal sandwiched between two gold electrodes and a fundamental frequency of 5 MHz, was utilized to evaluate the signal enhancement owing to the functionalized AuNPs. QCM-D can monitor in real-time shifts in wave frequency (ΔF) and energy dissipation (ΔD) of a material bound to the surface; ΔF is related to mass deposition and ΔD is related to the viscoelastic behavior of the adsorbed molecules. Here, a Q-Sense Analyzer E4 (Biolin Scientific, Sweden) instrument and 5 MHz, 14 mm Cr/Au crystals (AWS SNS 000042A, AWSensors, Spain) were used. The Au sensor surface was cleaned with 2% v/v Hellmanex, rinsed with dH_2O and 70% v/v ethanol and finally treated under UV ozone for 30 min. The clean Au surface was coated with spikes in PBS (0.06 mg mL^{-1}, V = 50 μL) and blocked with 1% w/v BSA and 1% v/v human serum negative for spike Ab. Then, a rabbit monoclonal anti-spike antibody (0.1–50 nM), spiked in 1% v/v human serum, was added to the immunoassay surface. To study signal amplification, a suspension of AuNPs (OD 1) conjugated with a goat anti-rabbit IgG was added on each surface, and the acoustic response was monitored with QCM-D.

Clinical validation of the immunoassay using patient samples

Human serum samples were tested for their anti-spike Ab titers with the commercially available ELISA kit QuantiVac anti-S + RBD IgG (Euroimmun, Germany) using the ELISA automated system Euroimmun Analyzer I (Laboratory of Clinical Virology, Medical School, University of Crete). The microplate wells were coated with the recombinant S1 subunit including the receptor binding domain (RBD) of the spike protein. Quantification of S1-specific IgG Ab was performed using a 6-point calibration curve covering a range from 1 to 120 relative units (RU mL^{-1}). Samples yielding results above this analytical range were re-evaluated at a higher dilution. Positive and negative controls were included in each test run, wherein <8 RU mL^{-1} were considered negative, 8–11 RU mL^{-1} as borderline and ≥11 RU mL^{-1} as positive (QuantiVac guidelines).

Serum samples from N = 20 patients provided by the Laboratory of Clinical Virology (Medical School, University of Crete) were aliquoted and stored at −80 °C until use. For evaluation of the samples using the developed acoustic immuno-

assays, each serum sample was diluted 100 times in PBS (1% v/v), and a final injection of 60 μL was used. Finally, a suspension of AuNPs (OD 1, V = 50 μL) functionalized with goat anti-human IgG (Fc) secondary Ab was injected after the addition of the serum sample. The serum samples were tested on both spike/BSA and PLL/spike/Casein surfaces. Full validation was carried out using both the Love-SAW flow cell and capillary-based SAW fluidic setups.

Data analysis and statistics

Data analysis and graphing were performed using OriginPro 2024 (OriginLab Corporation, Northampton, MA, USA). Statistical analysis of patient samples was also conducted in OriginPro 2024, using the *Paired Comparison Plot* app. Differences among multiple grouped mean values were assessed using one-way ANOVA followed by Tukey's *post hoc* test. Statistical significance was defined as $p < 0.05$.

Results and discussion

Optimization of immunoassay and SAW experimental setup for Ab-testing

We first evaluated the sensitivity and usability of different experimental platforms employing the SAW device and various fluidics, measuring units and biorecognition surfaces. Initially, we tested two biorecognition layers to detect protein biomarkers. For the proof-of-principle, we used spike protein as the biorecognition molecule to detect anti-spike Ab, all in PBS (pH 7.4). In all cases, the phase and amplitude of the SAW device were monitored and used to derive quantitative information on the target analyte, here anti-spike Ab. Initially, we used the simplest possible approach, where spike protein, the biorecognition molecule, was physisorbed directly on the Au-device surface followed by BSA adsorption as a blocking agent (Fig. 3A). We also started by using a commercial polymeric fluidic cell (see Fig. 1B) and a benchtop measuring unit (SENSeOR) (Fig. 1C) to monitor the binding process. From the real-time graphs we calculated a ΔPh^{spike} = 10.87 ± 1.93° (Fig. 3B) and ΔA^{spike} = 0.18 ± 0.03 dB (Table S1). Moreover, a binding isotherm was obtained by monitoring the phase change during the addition of various Ab concentrations (1, 2, 5, 10, 50 and 100 nM) in 1% w/v BSA or 1% v/v serum to the spike-modified surface. From Fig. 3C we calculated apparent affinity constants of K_D = 6.1 ± 1.0 nM and 5.0 ± 1.3 nM, respectively. Moreover, Fig. 3D proves that the binding of anti-spike Ab to the spike-modified Au surface is specific, as indicated by the low response obtained upon the addition of a non-specific Ab (anti-Interleukin) to the same surface (ΔPh = 0.13 ± 0.04°) or of anti-spike Ab to a BSA-modified surface (ΔPh = 0.08 ± 0.04°). Fig. 3D shows that the limit of detection of this assay is in the range of 1 nM, in agreement with previous studies.[24,40] The formation of the physisorbed spike-modified SAW surface is a simple process giving quite reproducible results. However, to reuse the device surface, treatment under UV ozone and cleaning with a detergent solution (Hellmanex) were necessary. Chemical treatment was also required for cleaning the Love-SAW fluidic cell before reusing in another experiment.

Further improvements in the detection system focused on the development of a biorecognition surface that could be easily cleaned and reused, ideally outside a dedicated laboratory. A PLL polymer layer was tested as a potential surface to attract the spike protein (Fig. 3E) but also as a layer that can be easily removed to regenerate the Au surface (rubbing with a cotton swab).[34] PLL has been used as a surface coating, as it is cationic in a neutral pH solution and promotes electrostatic attraction with the negatively charged surfaces of biomolecules.[41] PLL found in the form of a copolymer with grafted PEG units, named PLL-*g*-PEG, has been used as a surface coating to attract negatively charged DNA molecules from complex media (such as milk) and repel proteins.[42] Also, PLL-*g*-PEG coating was used to bind various concentrations of DNA molecules and thus check the sensitivity of the SAW devices to detect biomolecules.[34,43]

In this work, we initially combined the PLL-SAW approach with our in-house produced portable measuring unit (Fig. 1D), together with the commercial flow cell (Fig. 1B). Based on our protocol, spike protein (in PBS) was attached to a pre-adsorbed PLL layer on the SAW device, followed by casein addition. Casein was selected instead of BSA due to its better blocking performance on this surface (Fig. S2B). The formation of the PLL layer on the Au-coated device surface resulted in a phase change ΔPh^{PLL} = 1.02 ± 0.2° (Fig. 3F and Table S1) and a near zero amplitude response, in agreement with previous studies[44,45] and suggestive of a flat, tightly adsorbed layer;[42,46] a similar result was obtained when paper-based fluidics was used instead of the commercial one (Table S1).

Regarding the adsorption of spike protein (using commercial AWS fluidics) on PLL and on Au, changes of ΔPh^{spike}_{PLL} = 7.34 ± 0.80° and ΔPh^{spike}_{Au} = 10.87 ± 1.93° were recorded (Fig. 3F and Table S1), indicating a little less binding on the PLL than on the Au surface; the use of the paper-based fluidics resulted in an even (slightly) smaller coverage of 5.92 ± 0.36° on PLL. The corresponding calculation of the acoustic ratios[46] $(\Delta A/\Delta Ph)^{spike}$ gave values of 0.017 ± 0.004, 0.030 ± 0.004 dB and 0.061 ± 0.010 dB per deg respectively (Table S1).

Fig. 3G shows the binding isotherms of the anti-spike Ab on the pre-adsorbed spike protein as a function of the Ab concentration (with the commercial fluidics). Measuring the affinity of the reaction on the two surfaces (Fig. 3A and E), we found that this was slightly lower on the PLL (K_D^{PLL} = 10.9 ± 1.1 nM) than on the Au surface (K_D^{Au} = 5.0 ± 1.3 nM), most likely due to the different packing, orientation and even conformation of the spikes on the two surfaces. Inspection of the above-mentioned phase changes and acoustic ratios for spikes shows that the protein is more sparse and has a higher acoustic ratio on PLL indicative of a more extended structure.[47] On the other hand, the physisorbed molecules (spike on Au) are tightly bound and in a flatter mode/orientation (on average), as suggested by the lower acoustic ratio. The binding on PLL probably orients most of the spike molecules away from the

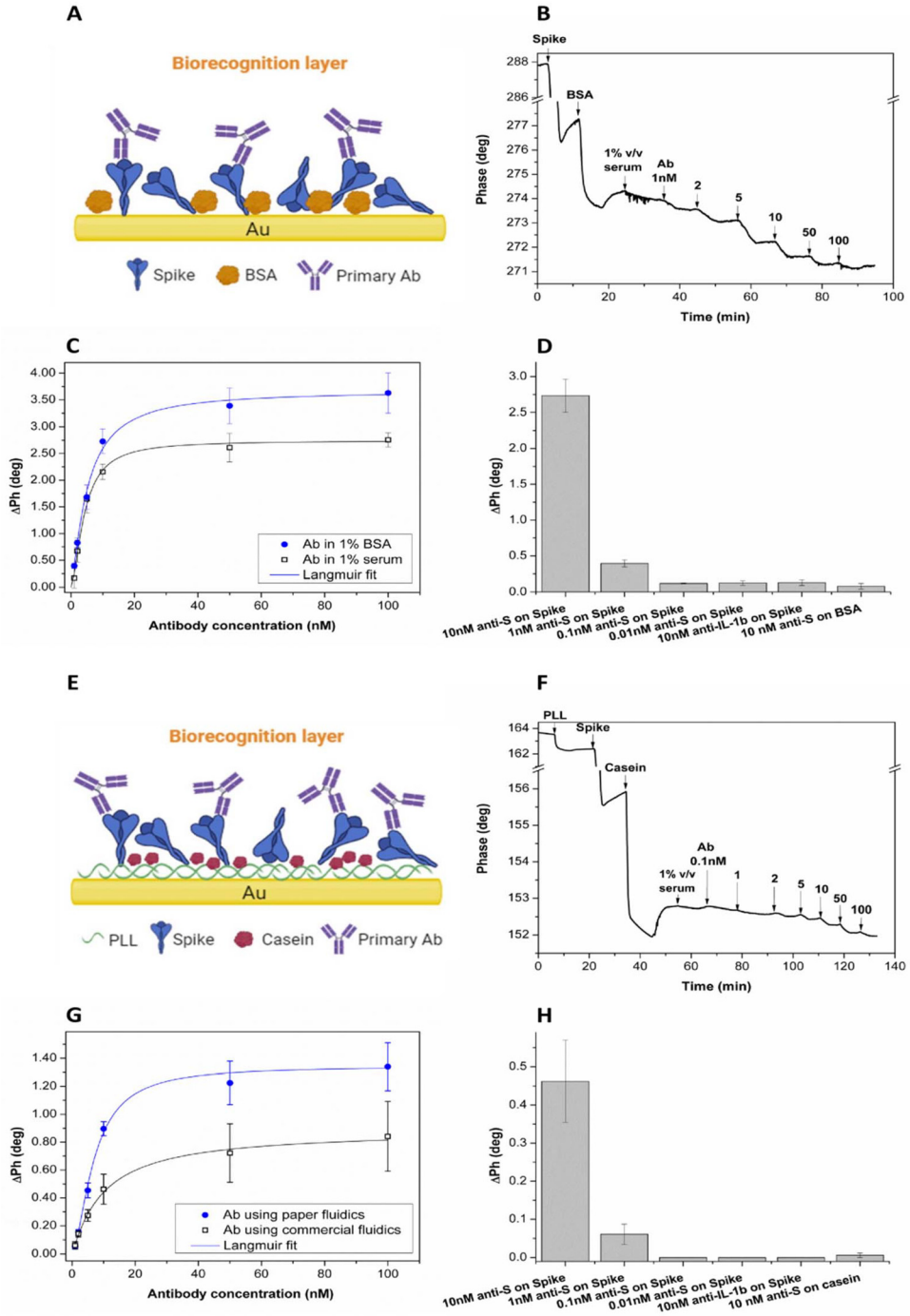

Fig. 3 (A) Schematic of the biorecognition layer consisting of spike protein adsorbed on the Au surface, BSA blocking and target antibody. (B) Real-time phase signal change during the binding of 1–100 nM anti-spike Ab in 1% v/v serum on the spike/BSA surface. (C) Binding isotherms of the target anti-spike Ab in 1% v/v serum (black squares) or 1% w/v BSA (blue circles) as a function of the antibody concentration using commercial (AWS) Love-SAW fluidics (spike/BSA surface). (D) Selectivity of anti-spike Ab on the spike/BSA surface; the binding of 10 nM anti-interleukin-1b Ab on the spike protein is also presented. (E) Schematic of the biorecognition layer consisting of PLL adsorbed on the Au surface, spike protein, casein blocking and target antibody. (F) Real-time phase signal change during the binding of 0.1–100 nM anti-spike Ab on the PLL/spike/casein surface. (G) Binding isotherm of the target anti-spike Ab in 1% v/v serum as a function of antibody concentration using commercial (AWS) (black squares) and paper fluidics (blue circles), *i.e.*, with the spike protein on PLL and casein as the blocking agent. (H) Selectivity of anti-spike Ab on the PLL/spike/casein surface; the binding of 10 nM anti-interleukin-1b Ab on the PLL/spike/casein surface is also presented. Note: schematics (A) and (E) were created with BioRender.com. The proteins are drawn approximately to scale; the dimensions are: IgG ~ 15 × 8 nm, BSA ~ 7 nm, casein ~ 3 nm and spike ~ 20 × 13 nm (at its RBD end).[53]

surface (protruding), also allowing more flexibility and stronger hydrodynamic coupling,[47] as suggested by the almost 2 to 4-fold increase of the acoustic ratio.[46] We conclude that both the Au and the PLL surfaces correctly orient (in different fractions) the spike (prolate shaped) molecule at the sensor's surface and also preserve its integrity, resulting in affinities (~5–10 nM) well within the range of published values, *i.e.* ~1–40 nM.[48,49]

Finally, we tested a configuration where the PLL surface was combined with the capillary paper fluidics and the portable measuring unit (Fig. 2A). The disposable paper strip enables liquid flow based on the capillary effect while continuous flow is maintained using a micropump. Fig. 3G shows that the binding isotherm obtained with the paper fluidics results in a larger phase response compared to the fluidic cell. This can be attributed to the larger sensing area and probably higher sensitivity in the case of the contactless paper fluidics compared to the surface-attached Love-SAW-chamber. However, in both cases, the detection limit was ~1 nM (Fig. 3D and H). The affinity constant here is K_D^{PLL} = 9.8 ± 2.5 nM, almost identical to the 10.9 nM value for the commercial arrangement. Finally, as before, we confirmed the specificity of the binding by recording negligible phase changes (~0.006°) when a non-specific Ab (anti-interleukin) was applied to spike or anti-spike Ab on a casein-modified PLL surface (Fig. 3D and H).

Overall, these results indicate that while differences may occur in the amount of immobilized spike protein and/or the subsequent affinity to the target anti-spike Ab, depending on the selected immobilization surface, in all tested cases the limit of detection is the same and in the low nM range.

Comparison of the SAW immune-assay with QCM technology – AuNPs for signal amplification

Seeking confirmation of our previous results obtained with the Love-SAW device and our newly developed setups, we employed a commercially available QCM acoustic device and QCM-D measuring technology as a benchmark. We studied the sensitivity of the QCM-D towards the detection of anti-spike Ab to the spike-modified gold-QCM surface, using 1% w/v BSA and 1% v/v serum solutions as blocking agents in PBS (Fig. 4A and B), as we did earlier. Fig. 4C and D show that the frequency (equivalent to phase) and dissipation (equivalent to amplitude) signals were both sensitive towards Ab binding within the concentration range of 0.1 to 50 nM, with ~1 nM again being the limit of detection. These results reassured us that the response obtained with our new hand-held SAW measuring unit and paper-based fluidics is equivalent to those obtained with a commercial lab-based standard instrument. Then, we examined the possibility for signal enhancement and hopefully LoD improvement by the use of (AuNPs). For this reason, we synthesized (using the Turkevich method) and fully characterized (Fig. S1) ~13 nm AuNPs functionalized with a secondary antibody "2Ab" (goat anti-rabbit IgG) able to bind to the Fc fragment of the primary anti-spike Ab. The AuNP-2Ab complexes exhibited almost zero non-specific binding to the spike/BSA surface and also to bound serum components; when target antibodies were added in the serum medium, they became readily detected by AuNP-2Ab complexes (Fig. 4B). In contrast to the previous results, in this case the dissipation was more sensitive than the frequency response giving a detection limit of 100 pM (instead of 1 nM) upon signal enhancement (Fig. 4C and D); this was also the case in a previous work where liposomes were used as the signal-enhancement particle.[50] The saturation of both frequency and dissipation signals at $[Ab]^{AuNPs} \approx 50$ nM is attributed to surface saturation with the AuNPs of OD 1 used in these experiments. It is generally accepted that acoustic wave phase changes relate well with surface-attached mass changes for both specific and non-specific interactions; it has also been shown that, in the case of specific binding, the phase change correlates well with the actual M_w of the molecule.[51] For our detection purposes, future work could then test the possibility of increasing the sensitivity of the assay by use of AuNPs with diameters greater than 13 nm.

With this promising result in hand, we subsequently used a similarly biofunctionalized probe (13 nm AuNPs with goat anti-human secondary antibody) with the Love-SAW experiments to amplify the signal of the immunoassay this time with clinical samples.

Validation of the SAW platform with patient samples

The Love-SAW acoustic setups were further tested using human serum samples already classified as positive or negative for anti-spike Ab using ELISA. Initially, we tested the response of the SAW biosensor to the addition of serum samples from patients negative to anti-spike Ab on the two bio-recognition surfaces. When negative serum was added directly to the Au-physisorbed spike protein surface (Fig. 3A), a high non-specific response was obtained (ΔPh = 0.33 ± 0.03°, Fig. S2A), probably due to partial surface-covering of the BSA leaving bare-Au areas. In the absence of spike antigens on a PLL/BSA-modified surface, a negative serum sample resulted in a ΔPh = 0.37° (Fig. S2B, black line). Again, the non-specific binding of BSA was high, potentially affecting the discrimination among the serum samples. This suggests that a Vroman-like effect is involved with the heavy serum proteins displacing the surface bound BSA molecules.[52] Therefore, alternatives for blocking layers were examined; casein turned out to be an excellent blocker, giving near-zero non-specific signals, for either 1% v/v negative serum or 1% w/v BSA solutions (Fig. S2B, blue line). A possible reason for the increased blocking capacity of casein could be the small size of the molecule, allowing it to be better entangled into the PLL polymer mesh. The PLL/casein-modified surface minimized the non-specific binding of negative human serum samples (ΔPh = 0.015 ± 0.029°) (Table S2). This observation is an indication that the PLL/casein combination provides a better surface than the Au/BSA one. For this reason, only the PLL/spike/casein surface was employed in our pilot clinical validation studies.

For our valuation studies, we tested a total of 20 clinical samples, 4 negative and 16 positive (ELISA-confirmed) on a PLL/spike protein modified surface (Fig. 3E), initially using the

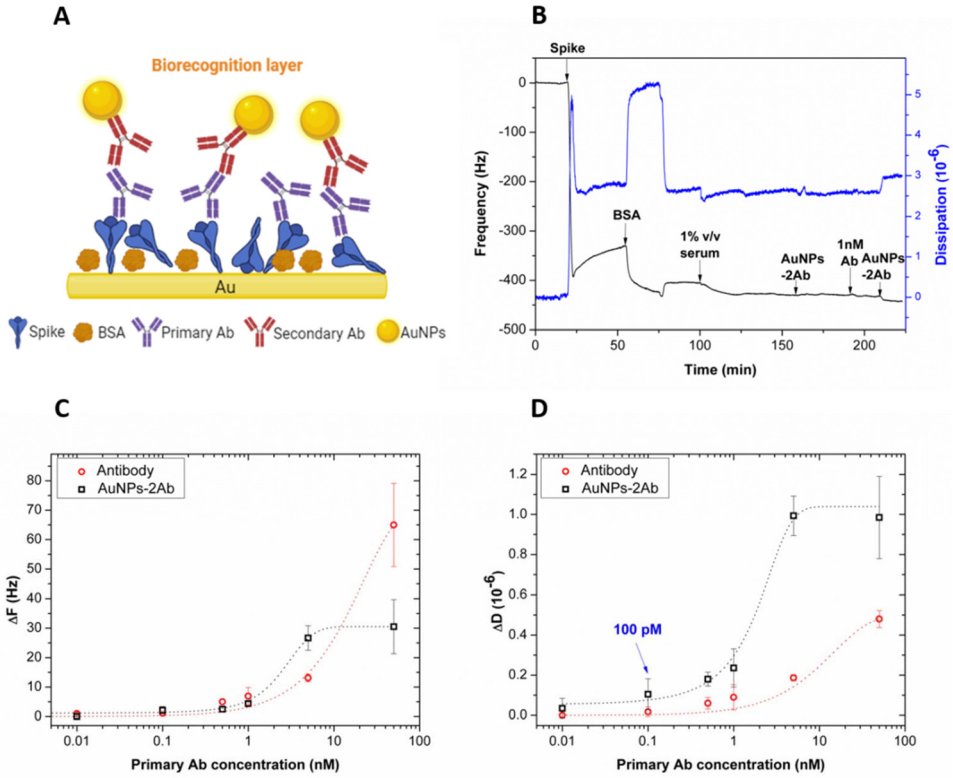

Fig. 4 (A) Schematic of the biorecognition layer consisting of spike protein adsorbed on the Au surface, BSA blocking agent, target antibody and AuNPs-2Ab complex bound on the target antibody. (B) Real-time frequency (black line) and dissipation (blue line) signals of spike adsorption on Au and blocking with BSA and 1% v/v human serum, followed by sequential addition of AuNPs-2Ab, 1 nM anti-spike Ab and AuNPs-2Ab. (C & D) Frequency and dissipation changes of primary anti-spike Ab binding on the spike/BSA surface (red circles) and the subsequent binding of AuNPs-2Ab able to bind to anti-spike Ab (black squares) as a function of the anti-spike Ab concentration (N = 3–5); the LoD is ~100 pM. Since the x-axis is in the logarithmic scale, the Ab concentration of 0.01 nM refers to the control measurement of 0 nM Ab added. All results reported here correspond to the 7th harmonic overtone and are used as raw numbers (*i.e.*, without dividing them by the overtone). Note: schematic (A) was created with BioRender.com. Like proteins, the AuNPs are drawn approximately to scale (~13 nm diameter).

Love-SAW commercial flow cell. To further improve the sensitivity of the assay, we again used the AuNPs for signal amplification and measured the corresponding ΔPh and ΔA. As before, AuNPs were functionalized with a secondary Ab that could bind to the Fc region of the anti-spike primary Ab found in human serum. As observed in Fig. 5A and B, the phase and amplitude responses of the SAW device in combination with the AuNP enhancement step can detect not only the positive samples but also differentiate them as low (11–116 RU mL^{-1}), mild (140–530 RU mL^{-1}) or strong (>1000 RU mL^{-1}) positive, depending on the Ab concentration in the sample. Moreover, from the same graphs we observe that the use of AuNPs can result in a 2 to 3 times larger phase and amplitude signals, respectively, compared to the direct assays, with the amplitude signal being more sensitive than the phase, in agreement with QCM results (Fig. 4D). This is confirmed by the ANOVA analysis, where the statistical difference at probability values between the different categories is improved in all cases when AuNPs are applied. Table S2 summarizes the acoustic signal values measured and used in Fig. 5A and B. The biosensor also showed excellent reproducibility when 3 representative human serum samples (one from each category) were tested 10 times each (Fig. S3 and Table S3). Finally, SEM micrographs of the SAW electrode surface after each functionalization step further verified the successful sequential modification of the biosensor surface (Fig. S4).

Moreover, some of these 20 clinical samples were also tested on the same PLL/spike coated SAW surface with the paper-based fluidics. Real-time graphs present the acoustic signal response obtained when one negative and three positives for anti-spike Ab patient samples were tested on the PLL/spike/Casein surface followed by signal amplification using the AuNPs-2Ab complex (Fig. 5C and D). Table S4 summarizes the acoustic signal values presented in Fig. 5C and D. As before, the use of the AuNPs resulted in a significant enhancement of both phase and amplitude signals, providing results in less than ~30 min. Plotting the changes in phase and amplitude as a function of the Ab concentration (RU mL^{-1}) shows that ΔA has an LoD of 47 RU mL^{-1} which is 1.7 times lower than the corresponding ΔPh LoD (78 RU mL^{-1}) (Fig. 5E and F). Compared to different biosensing technologies for the detection of anti-spike antibodies against SARS-CoV-2 (Table S5), the developed portable Love-SAW biosensor, particularly when combined with AuNPs as signal amplification

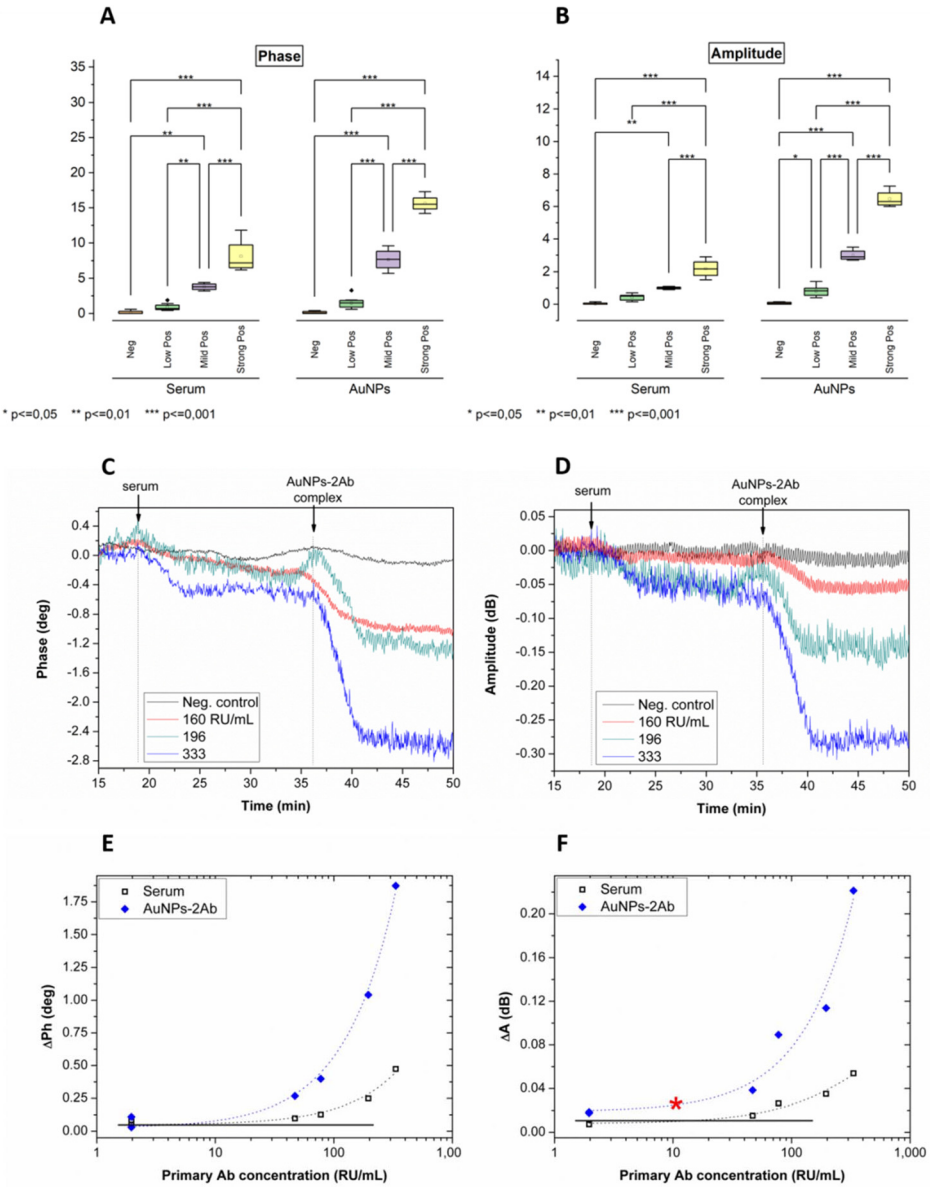

Fig. 5 (A) Phase and (B) amplitude signals obtained upon the addition of serum samples on a PLL/spike surface during direct and amplified assays using AuNPs-2Ab, tested with the commercial polymeric fluidic cell. (C) and (D) Real-time phase and amplitude signals, respectively, upon the addition of human serum samples directly and with AuNPs-2Ab for signal enhancement, both using the paper-based fluidics. (E) Phase and (F) amplitude signals, respectively, obtained from human serum samples (N = 6) and tested with the paper-based fluidics, without (black) and with (blue) AuNP-2Ab amplification. The asterisk (*) in (F) indicates the "clinical" limit between positive and non-positive samples (~11 RU mL^{-1}).

probes, demonstrates robust performance, good sensitivity, and rapid response. Moreover, the integration of real-time detection, a regeneratable biosensing surface and paper-based fluidics contributes to a simplified and portable platform suitable for point-of-care use.

Conclusions

The need to develop methods for testing outside a centralized laboratory calls for simple and fast assays combined with easy-to-use and cost-effective technologies. Acoustic devices can potentially offer a powerful biosensing element for such applications due to their proven capabilities and wide availability in the electronics industry. However, while the SAW devices are produced in large yields, their cost is prohibitive for making them a disposable part of a testing platform. The same applies to the standard polymeric flow cells normally employed for liquid handling, which require rigorous cleaning between experiments. Here, we addressed both challenges by employing a reusable SAW-device biorecognition surface and a disposable fluidic paper strip. The flexibility of the proposed on-the-

spot PLL-cleaning and surface regeneration method makes the PLL surface an attractive solution for field-based applications without compromising the quantitative capability of the sensor (1–100 nM). Combined with casein as the blocking agent, the PLL-adsorbed spike protein was proven to be well suited for the detection of Ab from patient samples, giving a negligible non-specific response in the presence of serum alone. Adding AuNPs for signal amplification during the detection of anti-spike Ab in serum resulted in a 3 times higher amplitude response, allowing discrimination between low (11–116 RU mL^{-1}), mild (140–530 RU mL^{-1}) and strong (>1000 RU mL^{-1}) titers using patient samples. The report of our novel paper-strip technology as a reusable fluidic module and our portable measuring unit complements previous studies where SAW biosensing devices and platforms were used as immunosensors. Specifically, a comparative study between the described setup and standard SAW or QCM platforms indicates that the assay performance is not affected by the mechanical/electrical parts applied for sample handling and acoustic detection. However, the user-friendliness, cost and capability for decentralized testing are significantly improved in the case of the paper-based capillary fluidics and portable measuring unit, allowing the development of a quantitative immunosensor for Ab detection near or at the point-of-care. Moreover, the disposable paper fluidic structure introduces, for the first time, the concept of affordable, robust, user-friendly and easy to deliver SAW fluidics in acoustic detection.

Author contributions

D. Chronaki: methodology, data curation, formal analysis, investigation, visualization, and writing – original draft. S. Grammatikos: methodology, data curation, formal analysis, investigation, visualization, and writing – review & editing. A. Ntimtsas: conceptualization, data curation, investigation, visualization, and methodology. M. Matsis: data curation, investigation, and visualization. O. F. Kokolakis: data curation, investigation, and visualization. K. Alexaki: data curation, investigation, and visualization. Z. Pournara: investigation and resources. A. Tsortos: validation and writing – review & editing. A. Zafiropoulos: resources and validation. E. Gizeli: conceptualization, funding acquisition, project administration, supervision, validation, and writing – review & editing.

Conflicts of interest

There are no conflicts to declare.

Ethical approval

The human serum samples were provided by the Virology Laboratory of the Medicine Department of the University of Crete and were fully anonymized (according to GDPR). The researchers involved in this study prepared and submitted the necessary documents to the Ethics and Research Integrity Committee of the University of Crete and obtained ethical approvals for working with patient samples (protocol number 118 13/5/2020).

Data availability

All data underpinning this study are available in the article and its supplementary information (SI). Supplementary information is available. See DOI: https://doi.org/10.1039/d6an00114a.

Acknowledgements

The authors would like to acknowledge Dr I. Reviakine for fruitful discussions and assistance during the development of the acoustic immunoassay and Ms. A. Manousaki (IESL-FORTH) and Ms. S. Papadogiorgaki (Electron Microscopy Lab, University of Crete) for their assistance in capturing SEM and TEM images, respectively.

The research project was supported by the European Union (EU) through the HORIZON-WIDERA-2023-ACCESS-07 – Excellence Hub Call (grant no. 101186531, project acronym "DxHub") and the Hellenic Foundation for Research and Innovation (H.F.R.I.) under the 4th Call for Action "Science and Society"-Emblematic Action - "Interventions to address the economic and social effect of the COVID-19 pandemic" (Project No.: 4969).

References

1 M. Zarei, *TrAC, Trends Anal. Chem.*, 2017, **91**, 26–41.
2 E. Fu, P. Yager, P. N. Floriano, N. Christodoulides and J. T. McDevitt, *IEEE Pulse*, 2011, **2**, 40–50.
3 A. K. Yetisen, M. S. Akram and C. R. Lowe, *Lab Chip*, 2013, **13**, 2210.
4 H.-C. Foreman, *Microbiol. Spectrum*, 2025, **13**, DOI: 10.1128/spectrum.01887-25.
5 L. Spicuzza, D. Campagna, C. Di Maria, E. Sciacca, S. Mancuso, C. Vancheri and G. Sambataro, *AIMS Microbiol.*, 2023, **9**, 375–401.
6 A. Riezk, V. Vasikasin, R. C. Wilson, T. M. Rawson, A. E. G. Cass and A. H. Holmes, *Sci. Rep.*, 2025, **15**, 24398.
7 Z. Li, H. Chen and P. Wang, *Analyst*, 2019, **144**, 3314–3322.
8 L. M. Rey Gomez, R. Hirani, D. W. Inglis, A. Care and Y. Wang, *Sens. Bio-Sens. Res.*, 2025, **50**, 100900.
9 K. Omidfar, F. Riahi and S. Kashanian, *Biosensors*, 2023, **13**, 837.
10 E. Lamprou, P. M. Kalligosfyri and D. P. Kalogianni, *Biosensors*, 2025, **15**, 68.
11 L. Bezinge, C. Shih, D. A. Richards and A. J. deMello, *Small*, 2024, **20**, DOI: 10.1002/smll.202401148.

12 X. Ying, W. Fu, L. Zhu, T. Sun, M. Qi, L. Zhou, Y. Wang, J. Wang, B. Su and J. Zhang, *Anal. Chem.*, 2024, **96**, 10630–10638.
13 V. Abarintos, A. Piper and A. Merkoci, *Curr. Opin. Electrochem.*, 2025, **54**, 101750.
14 K. Tsougeni, G. Kaprou, C. M. Loukas, G. Papadakis, A. Hamiot, M. Eck, D. Rabus, G. Kokkoris, S. Chatzandroulis, V. Papadopoulos, B. Dupuy, G. Jobst, E. Gizeli, A. Tserepi and E. Gogolides, *Sens. Actuators, B*, 2020, **320**, 128345.
15 A. Kordas, G. Papadakis, D. Milioni, J. Champ, S. Descroix and E. Gizeli, *Sens. Bio-Sens. Res.*, 2016, **11**, 121–127.
16 X. Ding, P. Li, S.-C. S. Lin, Z. S. Stratton, N. Nama, F. Guo, D. Slotcavage, X. Mao, J. Shi, F. Costanzo and T. J. Huang, *Lab Chip*, 2013, **13**, 3626.
17 K. Mitsakakis, A. Tserepi and E. Gizeli, *J. Microelectromech. Syst.*, 2008, **17**, 1010–1019.
18 M. Aleixandre and M. C. Horrillo, *Biosensors*, 2025, **15**, 88.
19 C.-H. Cheng, H. Yatsuda, M. Goto, J. Kondoh, S.-H. Liu and R. Wang, *Biosensors*, 2023, **13**, 605.
20 Y. Zeng, R. Yuan, H. Fu, Z. Xu and S. Wei, *RSC Adv.*, 2024, **14**, 37087–37103.
21 E. R. Gray, V. Turbé, V. E. Lawson, R. H. Page, Z. C. Cook, R. B. Ferns, E. Nastouli, D. Pillay, H. Yatsuda, D. Athey and R. A. McKendry, *npj Digit. Med.*, 2018, **1**, 35.
22 K. Toma, K. Oishi, N. Yoshimura, T. Arakawa, H. Yatsuda and K. Mitsubayashi, *Talanta*, 2019, **203**, 274–279.
23 Y.-C. Peng, C.-H. Cheng, H. Yatsuda, S.-H. Liu, S.-J. Liu, T. Kogai, C.-Y. Kuo and R. Y. L. Wang, *Diagnostics*, 2021, **11**, 1838.
24 V. Turbé, E. R. Gray, V. E. Lawson, E. Nastouli, J. C. Brookes, R. A. Weiss, D. Pillay, V. C. Emery, C. T. Verrips, H. Yatsuda, D. Athey and R. A. McKendry, *Sci. Rep.*, 2017, **7**, 11971.
25 C.-H. Cheng, Y.-C. Peng, S.-M. Lin, H. Yatsuda, S.-H. Liu, S.-J. Liu, C.-Y. Kuo and R. Y. L. Wang, *Biosensors*, 2022, **12**, 599.
26 Y. Jiang, C. Y. Tan, S. Y. Tan, M. S. F. Wong, Y. F. Chen, L. Zhang, K. Yao, S. K. E. Gan, C. Verma and Y.-J. Tan, *Sens. Actuators, B*, 2015, **209**, 78–84.
27 K. Toma, D. Miki, N. Yoshimura, T. Arakawa, H. Yatsuda and K. Mitsubayashi, *Sens. Actuators, B*, 2017, **249**, 685–690.
28 J. Lee, Y.-S. Choi, Y. Lee, H. J. Lee, J. N. Lee, S. K. Kim, K. Y. Han, E. C. Cho, J. C. Park and S. S. Lee, *Anal. Chem.*, 2011, **83**, 8629–8635.
29 J. J. Taylor, K. M. Jaedicke, R. C. van de Merwe, S. M. Bissett, N. Landsdowne, K. M. Whall, K. Pickering, V. Thornton, V. Lawson, H. Yatsuda, T. Kogai, D. Shah, D. Athey and P. M. Preshaw, *Sci. Rep.*, 2019, **9**, 11034.
30 K. Mitsakakis and E. Gizeli, *Anal. Chim. Acta*, 2011, **699**, 1–5.
31 H. J. Lee, K. Namkoong, E. C. Cho, C. Ko, J. C. Park and S. S. Lee, *Biosens. Bioelectron.*, 2009, **24**, 3120–3125.
32 S. Sreejith, J. Ajayan, N. V. U. Reddy, V. T. Vijumon and M. Manikandan, *Measurement*, 2026, **258**, 119094.
33 C. Wang, C. Wang, D. Jin, Y. Yu, F. Yang, Y. Zhang, Q. Yao and G.-J. Zhang, *ACS Sens.*, 2020, **5**, 362–369.
34 A. Ntimtsas and E. Gizeli, *Sens. Actuators, A*, 2024, **378**, 115814.
35 J. V. García, M. I. Rocha, C. March, P. García, L. A. Francis, A. Montoya, A. Arnau and Y. Jimenez, *Procedia Eng.*, 2014, **87**, 759–762.
36 D. Rabus, J.-M. Friedt, S. Ballandras, G. Martin, E. Carry and V. Blondeau-Patissier, *IEEE Trans. Ultrason. Ferroelectr. Freq. Control*, 2013, **60**, 1219–1226.
37 M. F. Cuddy, A. R. Poda and L. N. Brantley, *ACS Appl. Mater. Interfaces*, 2013, **5**, 3514–3518.
38 J. Liu and Y. Lu, *Nat. Protoc.*, 2006, **1**, 246–252.
39 M. Rodahl, F. Höök, A. Krozer, P. Brzezinski and B. Kasemo, *Rev. Sci. Instrum.*, 1995, **66**, 3924–3930.
40 H.-W. Chang and J.-S. Shih, *Sens. Actuators, B*, 2007, **121**, 522–529.
41 A. Di Mauro, F. Mirabella, A. D'Urso, R. Randazzo, R. Purrello and M. E. Fragalà, *J. Colloid Interface Sci.*, 2015, **437**, 270–276.
42 G. Papadakis, P. Palladino, D. Chronaki, A. Tsortos and E. Gizeli, *Chem. Commun.*, 2017, **53**, 8058–8061.
43 N. Bellassai, R. D'Agata, A. Marti, A. Rozzi, S. Volpi, M. Allegretti, R. Corradini, P. Giacomini, J. Huskens and G. Spoto, *ACS Sens.*, 2021, **6**, 2307–2319.
44 S. Nilsson and N. D. Robinson, *Electrochim. Acta*, 2016, **196**, 629–633.
45 M. Westwood, A. R. Kirby, R. Parker and V. J. Morris, *Carbohydr. Polym.*, 2012, **89**, 1222–1231.
46 A. Tsortos, G. Papadakis, K. Mitsakakis, K. A. Melzak and E. Gizeli, *Biophys. J.*, 2008, **94**, 2706–2715.
47 A. Tsortos, G. Papadakis and E. Gizeli, *Anal. Chem.*, 2016, **88**, 6472–6478.
48 M. M. Schneider, M. Emmenegger, C. K. Xu, I. Condado Morales, G. Meisl, P. Turelli, C. Zografou, M. R. Zimmermann, B. M. Frey, S. Fiedler, V. Denninger, R. P. Jacquat, L. Madrigal, A. Ilsley, V. Kosmoliaptsis, H. Fiegler, D. Trono, T. P. Knowles and A. Aguzzi, *Life Sci. Alliance*, 2022, **5**, e202101270.
49 D. Wrapp, N. Wang, K. S. Corbett, J. A. Goldsmith, C.-L. Hsieh, O. Abiona, B. S. Graham and J. S. McLellan, *Science*, 2020, **367**, 1260–1263.
50 D. Milioni, P. Mateos-Gil, G. Papadakis, A. Tsortos, O. Sarlidou and E. Gizeli, *Anal. Chem.*, 2020, **92**, 8186–8193.
51 K. Mitsakakis, A. Tsortos and E. Gizeli, *Analyst*, 2014, **139**, 3918–3925.
52 Z. W. Richter-Bisson and Y. S. Hedberg, *Colloids Surf., B*, 2025, **255**, 114927.
53 D. R. Beniac, A. Andonov, E. Grudeski and T. F. Booth, *Nat. Struct. Mol. Biol.*, 2006, **13**, 751–752.